Stable Laser-Driven Proton Beam Acceleration from a Two-Ion-Species Ultrathin Foil

Tong-Pu Yu,[1,2] Alexander Pukhov,[1,*] Gennady Shvets,[3,4] and Min Chen[1,5]

[1]*Institut für Theoretische Physik I, Heinrich-Heine-Universität Düsseldorf, 40225 Düsseldorf, Germany*
[2]*Department of Physics, National University of Defense Technology, Changsha 410073, China*
[3]*Univ Texas Austin, Dept Phys, Austin, Texas 78712 USA*
[4]*Univ Texas Austin, Inst Fus Studies, Austin, Texas 78712 USA*
[5]*Accelerator Fusion Research Division, Lawrence Berkeley National Laboratory, Berkeley, California 94720, USA*

(Received 10 December 2009; published 4 August 2010)

By using multidimensional particle-in-cell simulations, we present a new regime of stable proton beam acceleration which takes place when a two-ion-species shaped foil is illuminated by a circularly polarized laser pulse. In the simulations, the lighter protons are nearly instantaneously separated from the heavier carbon ions due to the charge-to-mass ratio difference. The heavy ion layer expands in space and acts to buffer the proton layer from the Rayleigh-Taylor-like (RT) instability that would have otherwise degraded the proton beam acceleration. A simple three-interface model is formulated to explain qualitatively the stable acceleration of the light ions. In the absence of the RT instability, the high quality monoenergetic proton bunch persists even after the laser-foil interaction ends.

DOI: 10.1103/PhysRevLett.105.065002 PACS numbers: 52.38.Kd, 52.27.Ny, 52.35.Mw, 52.65.Rr

Plasma-based ion accelerators have attracted a lot of attention due to their potential applications for particle acceleration, medical therapy [1], proton imaging, and inertial confinement fusion [2]. An important goal is to develop sources of laser-driven protons for radiation therapy of deep-seated tumors [3]. Numerous experimental and theoretical studies have been devoted to producing such proton beams [4,5]. However, beam qualities such as collimation, energy spread (~20%), and peak energy (~58 MeV), are still unsatisfactory [5].

Recently, with the rapid development of the laser, ultraintense ultrashort ultraclean (3U) laser pulses and ultrathin solid targets have been exploited to investigate the ion acceleration. One of the most straightforward acceleration mechanisms, radiation pressure acceleration (RPA) [6], is being revisited. The first RPA experiment [7] showed a greatly improved beam quality of the protons. However, the ultrathin foil is very susceptible to the transverse instabilities [8], similar to Rayleigh-Taylor-like (RT) instability in inertial confinement fusion. It sets in at the very beginning of laser-foil interaction and develops at the unstable interface within a few laser cycles [9]. Gradually, the surface of the foil becomes corrugated by the laser radiation and the entire target is torn into many clumps and bubbles [8]. The final energy spectrum of the ions shows a quasiexponential decay with sharp cutoff energy. Unlike the electron acceleration in the bubble regime [10], a stable proton beam acceleration in the realistic three-dimensional (3D) geometry has not been demonstrated either theoretically or experimentally.

In this Letter, we report on a new regime of stable proton beam acceleration, where a two-ion-species ultrathin foil is illuminated by a circularly polarized laser pulse. We assume the heavier (lighter) ions to be carbons (protons), respectively. Particle-in-cell (PIC) simulations indicate that the RT instability only causes the spreading of the carbon ions. The protons, which are rapidly separated from the carbon ions, are ''buffered'' by the carbon ion cloud by riding on the stable proton-carbon interface. We demonstrate that, even though the RT-unstable carbon-vacuum interface is strongly deformed, the feedthrough of the RT instability into the RT-stable proton-carbon interface is small. In the absence of the RT instability, the compact proton layer remains well collimated even after the laser-foil interaction ends. In order to elucidate the detailed acceleration process, we first describe the results of 1D simulations. Discussion of the influence of the RT instability on the ion acceleration follows, backed up by 3D simulations.

When a relativistic laser pulse illuminates a two-ion-species foil with thickness of a few wavelengths, a collisionless shock wave is often excited and can efficiently accelerate the ions to high energies [11]. With the decreasing foil thickness, the laser radiation pressure competes with the shock wave and becomes strong enough to push the entire foil forward. As a result, the foil acceleration is dominated by the RPA. The critical foil thickness [12] can be approximately estimated by $L \sim (a/\pi)(n_c/n_e)\lambda$, where $a = eE_L/m_e c\omega$ is the dimensionless laser amplitude, m_e the electron mass, n_e the electron density, and n_c is the critical plasma density. c, ω, λ, and E_L are the light speed in vacuum, the laser frequency, wavelength and electric field, respectively. In the 1D RPA model, the target motion equation is governed by

$$\rho \frac{d(\gamma\beta)}{dt} = \frac{E_L^2}{2\pi c} \frac{1-\beta}{1+\beta}, \tag{1}$$

where $\rho = \sum_i m_i n_i L$ is the target areal mass density, m_i and n_i are the ion mass and density, $\beta = v/c$ is the target velocity and $\gamma = 1/\sqrt{1-\beta^2}$ is the relativistic factor. We

can see that the target dynamics is defined by the areal mass density, not the detailed foil composition. In principle, the heavier ions can be efficiently accelerated to the same velocity as the lighter protons and electrons.

We simulate the described mechanism using the PIC code VLPL [13]. The longitudinal length of the 1D simulation box is $x = 60\lambda$ sampled by 6×10^4 cells, enough to resolve the expected density spikes. Each cell contains 100 numerical macroparticles in the plasma region. The target is 0.1λ thick, located at $x = 10\lambda$ and composed of carbon ions and protons with the same number density $46.7n_c$, which gives the electron density $n_e = 320n_c$. A circularly polarized laser pulse with the wavelength $\lambda = 1.06\ \mu$m is incident on the target from the left boundary. The wave front of the laser arrives at the target surface at $t = 10T_0$, where $T_0 = \lambda/c$ is the laser cycle. The laser pulse is homogeneous in space but has a trapezoidal profile (linear growth—plateau—linear decrease) in time. The duration is $\tau_L = 10T_0\ (1T_0 - 8T_0 - 1T_0)$. The dimensionless laser amplitude $a = 100$ is chosen to satisfy the requirement of the optimal ion acceleration in Ref. [12].

Figure 1(a) shows the particle density distribution at $t = 20T_0$. In the initial stage, the laser pressure is transferred to the electrons, resulting in the charge separation [12]. Because carbons and protons are initially colocated, the protons experience a higher acceleration due to their higher charge-to-mass ratio (Z_i/m_i). The time for protons to separate from the carbon ions is approximately $t_{\mathrm{sep}} = \sqrt{2Lm_H/eE_L} = 2.5$ fs, which is so short that it can be considered instantaneous. Later on, the two ion species start experiencing very different acceleration field, as shown by the red dashed curve in Fig. 1(a). The considerably higher electric field inside the carbon layer compensates for carbon's lower Z_i/m_i ratio enabling them to catch up with the protons. Eventually, both species travel together, without separating any further. The entire foil acceleration proceeds until the end of the laser-foil interaction at $t = 35T_0$. Figure 1(b) exhibits the phase space distribution. We can see that the carbon ions fall back behind the protons, accompanied by a long low-density tail. The fact that both species show an obvious "spiral structure" [14] in phase space provides a direct evidence for the acceleration process described above.

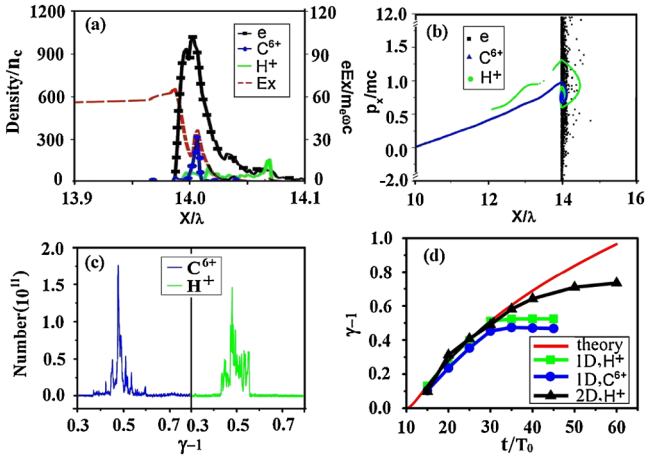

FIG. 1 (color online). (a) Density distribution of the electrons (black), protons (green), and carbon ions (blue) at $t = 20T_0$. The red dashed curve shows the electric field E_x, which is normalized to $E_0 = m_e c\omega/e = 3.2 \times 10^{12}$ V/m. (b) The corresponding phase space distribution at $t = 20T_0$. (c) Energy spectrum of the carbon ions (dark blue) and protons (light green) at $t = 30T_0$. (d) Energy evolution in time from PIC simulations and the 1D theory. The laser pulse is incident from the left side and touches the foil at $t = 10T_0$.

The ion energy spectrum is shown in Fig. 1(c). At $t = 30T_0$, the peak energy of the carbon ions is up to 480 MeV/u. For protons, all of them are accelerated to high energies although the energy spectrum is somewhat wider. Figure 1(d) plots the ion energy evolution. Here, we make use of the averaged energy for both species. At $t = 35T_0$, the laser-foil interaction ends so that the ion energy does not increase any more. Overall, the observed ion acceleration in the simulations is consistent with the prediction of the 1D theory above.

However, multidimensional simulations exhibit a radically different acceleration dynamics because multidimensional effects—such as transverse expansion of the bunch and the RT instability—come into play. In order to extend the 1D model to 2D simulations smoothly, we employ a shaped foil target (SFT) [15] to compensate for the transverse profile of the laser pulse. Taking the Gaussian laser, for example, the foil thickness should be matched transversely by the Gaussian function $L = \max[L_{\max} \exp(-y^2/\sigma_T^2), L_{\mathrm{cut}}]$, where $L_{\max}$ is the maximal foil thickness, L_{cut} the cutoff thickness, and σ_T the spot radius. In the following 2D case, the simulation box is $X \times Y = 80\lambda \times 32\lambda$, sampled by $16\,000 \times 400$ cells. The foil is initially located at $x = 10\lambda$ with parameters $L_{\max} = 0.1\lambda$, $L_{\mathrm{cut}} = 0.05\lambda$, and $\sigma_T = 7\lambda$. The carbon ion density is $51.9n_c$, intermingled with protons of the density $8.64n_c$ so that the total electron density is $320n_c$. A Gaussian laser pulse with the focal size $\sigma_L = 8\lambda$ is incident from the left boundary. All the other parameters are the same as in the 1D case.

Figure 2(a) shows the space distribution of the carbon ions and protons at different times. In each frame, the teal color marks the carbon ions and the red shows the protons. Obviously, the carbon ions behave totally different as compared with the 1D simulations. They spread widely in space and do not form a clear bunch. On the contrary, the protons from the center part of the foil always ride on the carbon ion front and form a compact bunch. The sharp front separating the two species is well defined and remains stable even after the laser-foil interaction ends. We can get a further understanding of the acceleration process from the phase space distribution, as shown in Figs. 3(a) and 3(b). On the one hand, the carbon ions evolve into a wide cloud in space. On the other hand, their front trails the protons so that the gap between the two species is always

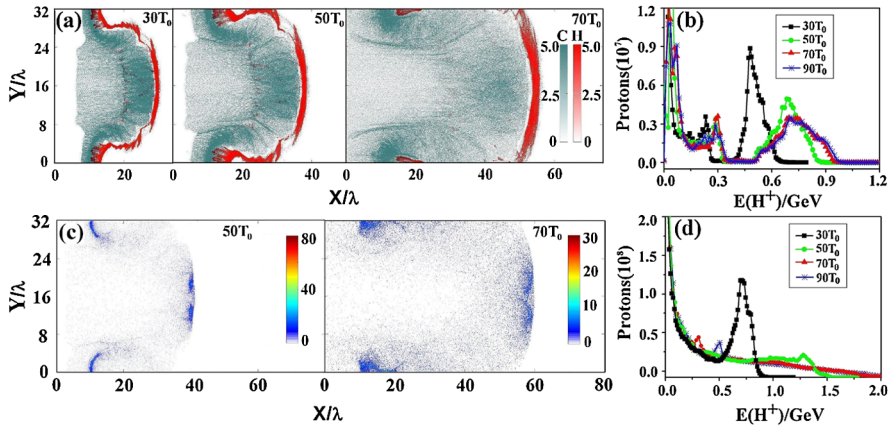

FIG. 2 (color online). (a) Contours of protons (dark red) and carbon ions (light teal) in the 2D case at different time points: $t = 30T_0$, $50T_0$, and $70T_0$. The color bar represents the proton numbers $\log(N)$. (b) Proton energy spectrum at: $t = 30T_0$ (square, black), $t = 50T_0$ (circle, green), $t = 70T_0$ (triangle, red), and $t = 90T_0$ (star, blue). For comparison, Frame (c) shows the proton density distribution in a pure hydrogen foil and frame (d) corresponds to its energy spectrum evolution.

small. The protons show a clear spiral structure, like a "matchstick," which coincides with the 1D simulations above. Figure 2(b) shows the proton energy spectrum. As expected, the peak is well pronounced and the dispersion is suppressed. The peak energy evolution is presented in Fig. 1(d), which is also in accordance with the predication of the 1D RPA model above. Figures 3(c) and 3(d) plot the ion energy-divergency distribution at $t = 30T_0$. The high quality proton bunch with the energy ~500 MeV and the opening angle ~5.5° forms and persists in time even after the laser-foil interaction ends.

The stability of the proton acceleration in the 2D simulations can be attributed to two effects. First, the protons rapidly separate from the carbon ions and form a thin shell, which is a prerequisite for stable proton acceleration. Such a separation of the ion species can be understood within the 1D formalism developed in Ref. [12] and the 1D simulation above. Second, the heating of the carbon ions forms an extended cloud that prevents short-wavelength perturbations of the surface from feeding through into the thin proton shell. We propose a simple three-interface model, as shown in Fig. 4(a), to explain the stabilization. In the accelerating reference frame of the foil, the perturbation pressure p satisfies

$$\frac{\partial^2}{\partial z^2}\delta p = -k_{\mathrm{RT}}^2 \delta p, \tag{2}$$

where k_{RT} is the wave number of the RT-unstable mode. Noting that δp is discontinuous across the unperturbed boundary, we obtain a solution $\delta p = A_i e^{-k_{\mathrm{RT}} z} + B_i e^{k_{\mathrm{RT}} z}$ away from interfaces, with A_i and B_i being the amplitude coefficients of the perturbation inside the layer consisting of the ith species. In our case, both species have two interfaces: one with vacuum and one with the other species. For the carbon ions ($i = \mathrm{C}$), the only unstable interface is the carbon-vacuum boundary, where the laser pulse interacts directly with the carbon plasma. We derive from the model that the amplitude of the perturbation is exponentially decaying away from the unstable interface:

$$\frac{A_{\mathrm{H}}}{A_{\mathrm{C}}} \sim e^{-k_{\mathrm{RT}} L_{\mathrm{C}}}, \tag{3}$$

where L_{C} is the thickness of the carbon ion layer. In the simulations, L_{C} is several times longer than L_{H} so that the perturbation in the carbon layer would take much more time to grow (recall that the growth rate of the RT instability $\gamma \propto \sqrt{g/\lambda_{\mathrm{RT}}}$, where g is the target's acceleration and λ_{RT} is the perturbation wavelength). The feedthrough from the unstable carbon-vacuum interface to the proton layer is exponentially attenuated according to Eq. (3). This simple qualitative argument explains the stability of the sharp carbon-proton interface. For the thin proton layer, it is also stable because the protons are much lighter than the carbon ions. It is helpful to consider the problem from the purely hydrodynamic RT instability [16] which occurs when a light fluid is accelerated into a heavy fluid. Eventually, the entire proton layer is free from the RT

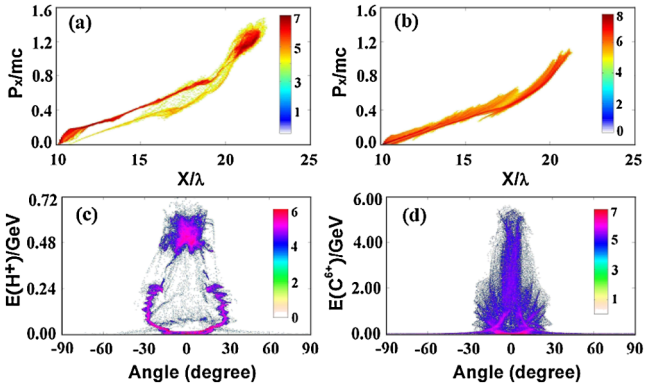

FIG. 3 (color online). Phase space of (a) protons and (b) carbon ions at $t = 30T_0$. An obvious spiral structure is observed only for protons. Frames (c) and (d) show the carbon ion and proton energy distribution as a function of the divergency angle at $t = 30T_0$.

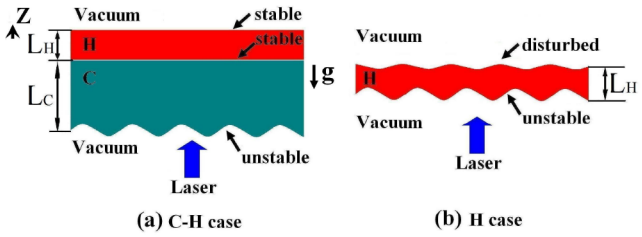

FIG. 4 (color online). Schematic of the laser-foil interaction in (a) C-H case and (b) pure H case. Here, $L_H \ll L_C$. In case (a), there are three interfaces: carbon-vacuum, carbon-proton, and proton-vacuum. Only the first interface is unstable. In case (b), both interfaces are finally unstable.

instability. Besides, we believe that the small transverse size of the foil also benefits the stabilization of the proton acceleration in this case. The minimal perturbation wave number can be estimated by $k_{RT} = 2\pi/Y$, where Y is the transverse foil size. At $t = 30T_0$, the carbon shell thickness is $L_C \approx 10\lambda$ and $Y = 32\lambda$. In this case, Eq. (3) already indicates a considerable suppression of the perturbation feedthrough.

Now we compare the stable multicomponent foil case with the pure hydrogen foil case, where the RT instability is obvious. We again employ a matched SFT. All the parameters are the same as above except now $n_H = 320n_c$ and the carbon ions are absent. Figure 2(c) shows the proton density distribution in space. We can see that the foil disrupts gradually and two proton bunches with a lower density valley in the middle form. This is very characteristic for the RT instability driven by the laser radiation. Using the linear stability theory of the accelerated foil [8], the growth time of the perturbation in the relativistic limit can be derived as the following:

$$\frac{\tau_{RT}}{T_0} = \frac{\sqrt{2}}{6}\sqrt{\frac{m_e}{m_i}\frac{n_c}{n_i}\frac{\lambda}{L}}\left(\frac{\lambda_{RT}}{\lambda}\right)^{3/2} a. \quad (4)$$

Taking into account $\lambda_{RT} \simeq \sigma_L = 8\lambda$ and $L = 0.1\lambda$ in our case, we estimate that the time scale of the instability should be $2.2T_0$. Such a short-wavelength perturbation grows very fast so that it reaches the other side of the foil soon, as shown in Fig. 4(b). Finally, both interfaces are unstable and the entire target collapses quickly. Figure 2(d) shows the proton energy spectrum. Although an energy peak is observed initially, it lowers gradually and disappears at $t = 45T_0$, leaving a quasiexponential spectrum. In fact, most single-ion foils in the RPA regime show a similar result [6,8,14,15]. The main issue is the fast growth of the short-wavelength perturbation at the unstable interface.

In order to check the robustness of the stable regime, we perform 3D simulations while keeping all the parameters same as in the 2D case except $\sigma_T = 6\lambda$. A stable structure of the proton beam acceleration is also observed, which indicates that the regime described above can significantly stabilize the proton beam acceleration in the realistic three-dimensional geometry.

In conclusion, we present a new regime of stable proton beam acceleration driven by the laser radiation pressure. In this regime, we smoothly extend the 1D RPA model to multidimensional cases by using a two-ion-species ultrathin SFT. PIC simulations show that the transverse instability degrades only the carbon ion acceleration and spreads them in space. The sharp front separating the two species is always stable so that the proton layer is free from the effects of the RT instability. Benefiting from the superpower lasers such as HiPER and ELI, this stable regime might open a new way to high quality proton beam generation in the near future.

This work is supported by the DFG programs GRK1203 and TR18. T. P. Y. acknowledges financial support from the China Scholarship Council and the NSAF program (Grant No. 10976031). G. S. acknowledges the support of the U.S. DOE Grants No. DE-FG02-05ER54840 and No. DE-FG02-04ER41321. M. C. acknowledges support from the Alexander von Humboldt Foundation.

*pukhov@tp1.uni-duesseldorf.de

[1] S. V. Bulanov *et al.*, Phys. Lett. A **299**, 240 (2002).
[2] T. Ditmire *et al.*, Nature (London) **398**, 489 (1999).
[3] A. R. Smith, Med. Phys. **36**, 556 (2009).
[4] B. M. Hegelich *et al.*, Nature (London) **439**, 441 (2006); D. Neely *et al.*, Appl. Phys. Lett. **89**, 021502 (2006); L. Willingale *et al.*, Phys. Rev. Lett. **96**, 245002 (2006); T. P. Yu *et al.*, Phys. Plasmas **16**, 033112 (2009); I. A. Andriyash *et al.*, Plasma Phys. Rep. **36**, 77 (2010).
[5] H. Schwoerer *et al.*, Nature (London) **439**, 445 (2006).
[6] A. P. L. Robinson *et al.*, New J. Phys. **10**, 013021 (2008); A. Macchi, S. Veghini, and F. Pegoraro, Phys. Rev. Lett. **103**, 085003 (2009); B. Qiao *et al.*, Phys. Rev. Lett. **102**, 145002 (2009); M. Chen *et al.*, New J. Phys. **12**, 045004 (2010); S. V. Bulanov *et al.*, Phys. Rev. Lett. **104**, 135003 (2010).
[7] A. Henig *et al.*, Phys. Rev. Lett. **103**, 245003 (2009).
[8] F. Pegoraro and S. V. Bulanov, Phys. Rev. Lett. **99**, 065002 (2007); S. V. Bulanov *et al.*, Eur. Phys. J. D **55**, 483 (2009).
[9] M. Chen *et al.*, Phys. Plasmas **15**, 113103 (2008).
[10] A. Pukhov and J. Meyer-ter-Vehn, Appl. Phys. B **74**, 355 (2002).
[11] L. Ji *et al.*, Phys. Rev. Lett. **101**, 164802 (2008); X. Zhang *et al.*, Phys. Rev. ST Accel. Beams **12**, 021301 (2009).
[12] V. K. Tripathi *et al.*, Plasma Phys. Controlled Fusion **51**, 024014 (2009).
[13] A. Pukhov, J. Plasma Phys. **61**, 425 (1999).
[14] A. Macchi *et al.*, Phys. Rev. Lett. **94**, 165003 (2005); X. Q. Yan *et al.*, Phys. Rev. Lett. **100**, 135003 (2008).
[15] M. Chen *et al.*, Phys. Rev. Lett. **103**, 024801 (2009); T. P. Yu *et al.*, Laser Part. Beams **27**, 611 (2009).
[16] L. Rayleigh, Proc. London Math. Soc. **s1-14**, 170 (1882); G. I. Taylor, Proc. R. Soc. A **201**, 192 (1950).